The Astrophysical Journal, 873:131 (16pp), 2019 March 10 https://doi.org/10.3847/1538-4357/ab05c4

Self-consistent Solutions for Line-driven Winds of Hot Massive Stars: The m-CAK Procedure

Alex C. Gormaz-Matamala[1,2], M. Curé[1,2], L. S. Cidale[3,4,5], and R. O. J. Venero[3,4]
[1] Instituto de Física y Astronomía, Universidad de Valparaíso, Av. Gran Bretaña 1111, Casilla 5030, Valparaíso, Chile; alex.gormaz@postgrado.uv.cl
[2] Centro de Astrofísica, Universidad de Valparaíso. Av. Gran Bretaña 1111, Casilla 5030, Valparaío, Chile
[3] Departamento de Espectroscopía, Facultad de Ciencias Astronómicas y Geofísicas, UNLP. Paseo del Bosque S/N, 1900 La Plata, Argentina
[4] Instituto de Astrofísica de La Plata, CCT La Plata, CONICET-UNLP. Paseo del Bosque S/N, 1900 La Plata, Argentina
Received 2018 June 29; revised 2019 January 30; accepted 2019 February 7; published 2019 March 13

Abstract

Massive stars present strong stellar winds that are described by the radiation driven wind theory. Accurate mass-loss rates are necessary to properly describe the stellar evolution across the Hertzsprung–Russel Diagram. We present a self-consistent procedure that coupled the hydrodynamics with calculations of the line-force, giving as results the line-force parameters, the velocity field, and the mass-loss rate. Our calculations contemplate the contribution to the line-force multiplier from more than ∼900,000 atomic transitions, an NLTE radiation flux from the photosphere and a quasi-LTE approximation for the occupational numbers. A full set of line-force parameters for $T_{\rm eff} \geqslant 32{,}000$ K, surface gravities higher than 3.4 dex for two different metallicities are presented, with their corresponding wind parameters (terminal velocities and mass-loss rates). The already known dependence of line-force parameters on effective temperature is enhanced by the dependence on $\log g$. The terminal velocities present a stepper scaling relation with respect to the escape velocity, this might explain the scatter values observed in the hot side of the bistability jump. Moreover, a comparison of self-consistent mass-loss rates with empirical values shows a good agreement. Self-consistent wind solutions are used as input in FASTWIND to calculate synthetic spectra. We show, comparing with the observed spectra for three stars, that varying the clumping factor, the synthetic spectra rapidly converge into the neighborhood region of the solution. It is important to stress that our self-consistent procedure significantly reduces the number of free parameters needed to obtain a synthetic spectrum.

Key words: hydrodynamics – methods: numerical – stars: early-type – stars: mass-loss – stars: winds, outflows

1. Introduction

The study of massive stars (i.e., stars with $M_* > 10\,M_\odot$) is a relevant topic in the framework of stellar astrophysics, because these stars exhibit some of the most extreme physical conditions, such as the hottest temperatures, the highest outflows of matter, and a complex nucleosynthesis.

Strong outflowing stellar winds of massive stars eject high amounts of matter that contribute to the chemical enrichment of the ISM in a relatively short timescale. Moreover, it has been found that differences on a factor of two in the mass-loss rate considerably affects the final fate of a star (Meynet et al. 1994; Smith 2014). Therefore, a better understanding about massive stars and their evolution strongly requires accurate determination of their fundamental parameters, with the mass-loss rate being the most relevant (Kudritzki & Puls 2000; Puls et al. 2008).

Lucy & Solomon (1970) described the mechanism that drives the strong stellar winds observed in hot stars: the so-called radiation driven winds. According to these authors, the absorption and further reemission of photons by UV resonance lines is the wind-driven mechanism for hot stars, that produces an outward line-force. The foundation of the theory of radiation driven winds was later developed by Castor et al. (1975, hereafter CAK theory), who, based on the Sobolev and the point-star approximations, modeled the line-acceleration analytically in terms of the acceleration produced by electron scattering times a force multiplier factor. This factor represents the contribution of absorption and reemission processes depending on the optical depth only, and it was parameterized by two constant parameters through the wind, namely k and α.

Later, Abbott (1982) performed a detailed calculation of these line-force parameters taking into account the contribution of a full set of atomic line transition data for elements from hydrogen to zinc. Due to the point-star approximation the derived hydrodynamical values for mass-loss rates were overestimated; Pauldrach et al. (1986) and Friend & Abbott (1986) relaxed this approximation and considered the finite-disk shape of the star. With this modified theory (hereafter m-CAK), they solved the equation of motion and obtained improved theoretical results, in better agreement with the observed mass-loss rates.

Due to scarce works concerning NLTE (nonlocal thermodynamic equilibrium) calculations of the line-force parameters (Pauldrach et al. 1986; Puls et al. 2000; Kudritzki 2002; Pauldrach 2003; Noebauer & Sim 2015), it was difficult to obtain from the m-CAK hydrodynamics the velocity profiles and mass-loss rates; thus, the massive star community started to use the so-called β-law velocity profile. This simplified description of the velocity field is widely used as input in radiative transfer and NLTE model-atmosphere codes such as FASTWIND (Santolaya-Rey et al. 1997; Puls et al. 2005) or CMFGEN (Hillier 1990; Hillier & Miller 1998; Hillier & Lanz 2001) to calculate synthetic spectra. In this procedure, stellar and wind parameters (terminal velocity and mass-loss rates) are treated as free and are determined by varying them to adjust synthetic to observed line profiles. Kudritzki & Puls (2000) argued that the use of β-law for the velocity field is only justified a posteriori

[5] Member of Carrera del Investigador Científico de CONICET, Argentina.

once the fit is achieved. There are other approaches that coupled the hydrodynamics with comoving frame radiative transfer, see, e.g., Sander et al. (2017) or Krtička & Kubát (2010, 2017), that do not use a β-law velocity profile.

Calculations of line-force wind parameters coupled with hydrodynamics are necessary to derive self-consistent velocity profiles and mass-loss rates. Moreover, they depend nonlinearly on the stellar parameters, chemical abundances, and atomic data via the wind-driven mechanism. To obtain the line-force parameters it is necessary to calculate the *total acceleration* produced by the contribution of hundreds of thousands of lines participating in the absorption and reemission processes (hereafter line-acceleration $g_{\rm line}$). Thus, having reliable atomic data is essential to perform *line-statistics* calculations.

The number of contributing lines to the driven line-acceleration depends on the wind opacity and it is strongly coupled to the wind density and velocity profiles. To solve this highly nonlinear problem an iterative procedure is required to satisfy both: line-statistics and m-CAK hydrodynamics.

In this work, we calculate self-consistent solutions to obtain accurate m-CAK line-force parameters (k, α, δ) and wind properties of hot massive stars. The hydrodynamics is provided using our code HYDWIND (Curé 2004), whereas abundances have been updated from Asplund et al. (2009). Final self-consistent line-force values correspond to a unique solution obtained when line-force parameters, velocity profile, and mass-loss rate converged. Hence, we present here a new set of m-CAK self-consistent line-force parameters for $T_{\rm eff} > 32{,}000$ K and $\log g \geqslant 3.4$, with the corresponding velocity profile and mass-loss rate. These line-force parameters are compared with previous numerical studies. Furthermore, with these new results we calculate synthetic spectra with FASTWIND contrasting them with observations. We show that applying few times our procedure we obtain a very good fit of the observed line profile. Furthermore, we derived (i) an alternative recipe for the mass-loss rate, which only depends on the stellar parameters and the abundance; (ii) the ratio $v_{\rm inf}/v_{\rm esc}$ as given by Equation (18) now depends not only on the line-force parameter α but also on $\log g$.

This paper is organized as follows: The theoretical formulation of m-CAK theory is given in Section 2. Section 3 describes the methodology used, explaining the iterative procedure and how convergence is assured. Section 4 shows results for the calculation of the line-force multiplier using the standard solution, together with a detailed analysis about under what conditions (k, α, δ) can be treated as constants. In Section 5, we calculate synthetic spectra based on our self-consistent procedure and compare them with observations. A discussion about the results is given in Section 6. Finally, our conclusions are presented in Section 7.

2. Theoretical Formulation

The m-CAK theory (Castor et al. 1975; Friend & Abbott 1986; Pauldrach et al. 1986) describes in spherical coordinates a stationary, nonrotating, expanding atmosphere, taking into account the line-acceleration $g_{\rm line}$. The equation of momentum and equation of continuity respectively read:

$$v\frac{dv}{dr} = -\frac{1}{\rho}\frac{dP}{dr} - \frac{GM_*(1-\Gamma_e)}{r^2} + g_{\rm line}, \tag{1}$$

and

$$\dot{M} = 4\pi\rho(r)r^2v(r). \tag{2}$$

Here, $\dot{M}$ is the mass-loss rate, $v(r)$ is the radial velocity field, $\rho(r)$ is the mass density, P is the gas pressure, and $M_*(1-\Gamma_e)$ corresponds to the effective stellar mass, where Γ_e is the radiative acceleration caused by Thomson scattering in terms of gravitational acceleration.

Introducing the following dimensionless variables: $\hat{r} = r/R_*$, $\hat{v} = v/a$, and $\hat{v}_{\rm crit} = v_{\rm esc}/a\sqrt{2}$, where the escape velocity is defined as $v_{\rm esc}^2 = 2\,G\,M_*\,(1-\Gamma_e)/R_*$. Then, the equation of motion reads:

$$\left(\hat{v} - \frac{1}{\hat{v}}\right)\frac{d\hat{v}}{d\hat{r}} = -\frac{\hat{v}_{\rm crit}^2}{\hat{r}^2} + \frac{2}{\hat{r}} + \hat{g}_{\rm line}, \tag{3}$$

with $\hat{g}_{\rm line} = (R_*/a^2)g_{\rm line}$. We have used the equation of state of an ideal gas, $P = a^2\rho$, with a being the isothermal sound speed:

$$a = \sqrt{\frac{k_B T_{\rm eff}}{\mu\, m_{\rm H}}}, \tag{4}$$

with μ being the mean atomic weight.

The line-acceleration can be defined in terms of the radiative acceleration due to electron scattering $\hat{g}_e = (R_*/a^2)g_e$, multiplied by $\mathcal{M}(t) = \hat{g}_{\rm line}/\hat{g}_e$, called the *line-force multiplier factor*. $\mathcal{M}(t)$ corresponds to the sum of spectral lines that contribute to drive the wind:

$$\mathcal{M}(t) = \sum_{\rm lines}\Delta\nu_D\,\frac{F_\nu}{F}\frac{1-e^{-\eta_{\rm line}\,t}}{t}, \tag{5}$$

with $\Delta\nu_D$ being the line broadening due to Doppler effects. F_ν and F are the monochromatic and total stellar flux, respectively, and $\eta_{\rm line}$ is the absorption coefficient. Castor (1974) parameterized $\mathcal{M}(t)$ in terms of the optical depth t, which depends on the wind structure only:

$$t = \sigma_e\,\rho(r)v_{\rm th}\left(\frac{dv}{dr}\right)^{-1}, \tag{6}$$

with $v_{\rm th}$ being the mean hydrogen thermal velocity.

Then, Castor et al. (1975) proposed the following analytical expression for $\mathcal{M}(t)$:

$$\mathcal{M}(t) = k\,t^{-\alpha}, \tag{7}$$

where the parameters k and α are the so-called *line-force multiplier parameters* (or line-force parameters). Abbott (1982) added a third line-force parameter called δ, being the exponent of the diluted-electron number density, N_e/W (where W is the dilution factor). With these three line-force parameters (k, α, δ), $\mathcal{M}(t)$ becomes:

$$\mathcal{M}(t) = k\,t^{-\alpha}\left(10^{-11}\frac{N_e}{W}\right)^{\delta}. \tag{8}$$

The physical interpretation of the line-force parameters (see, e.g., Puls et al. 2000) are as follows:

1. The k parameter is directly proportional to the effective number of driving lines, and is related to the fraction of the photospheric flux, which would have been blocked by all lines if they were optically thick and overlapping effects were not considered. Higher values of k are obtained at higher densities and, therefore, higher mass-loss rates. In addition to the dependency of $\rho(r)$, k presents also a strong dependence with metallicity and temperature due to the large number of driving lines: a

lower temperature implies lower ionization stages, and thus more lines; therefore, a higher $\mathcal{M}(t)$. More lines (above a given threshold line strength) are also present for higher metallicities.

The overlapping of two or more spectral lines produces an overestimation in the calculated value of k. On the other hand, k is underestimated when multiscattering effects are not taken into account (i.e., the summation in $\mathcal{M}(t)$ considers only direct photospheric radiation, and not radiation reprocessed in the wind). As was pointed out by Puls (1987), the inclusion of both effects might cancel, at least for O stars, and the *effective* k becomes moderately reduced. In this work, we have not considered these effects; therefore, our k values should be maximum.

2. The α parameter is related to the exponent of the line-strength distribution function, and quantifies also the ratio of the line-acceleration from optically thick lines to the total one (for details, see Puls et al. 2008).
3. The δ parameter represents the change in the ionization throughout the wind. It has been found that, high values of δ ($\gtrsim$0.25) "slow" the wind, yielding a different wind solution (Curé et al. 2011).

Some studies have pointed out that the line-force parameters are a function of radius (Schaerer & Schmutz 1994) or can be considered in a piecewise constant structure (Kudritzki 2002). Nevertheless, in this work, we will consider k, α, and δ as constants throughout the wind (see Section 4.2).

3. Calculation of the $\mathcal{M}(t)$ Factor

To calculate the $\mathcal{M}(t)$ factor, we include different improvements: (i) a larger line list, (ii) a quasi-NLTE approach for the ionization equilibrium, (iii) an NLTE radiative stellar flux, and (iv) an optical depth range in concordance with the wind structure. Then we test it for one single-step and also the whole iteration procedure until convergence of line-force parameters, velocity profile, and mass-loss rate is achieved.

3.1. Selection of Atomic Database

To calculate the line-acceleration and obtain a proper value of $\mathcal{M}(t)$, Abbott (1982) established that it is necessary to sum the contribution of hundreds of thousands of spectral lines participating in the line-acceleration processes. Therefore, aiming to get the most accurate value of $\mathcal{M}(t)$, we decided to employ around ~900,000 line transitions. These atomic data were obtained (and modified in format) from the atomic database list used by the code CMFGEN[6] (Hillier 1990; Hillier & Miller 1998). Specifically, we have extracted information related to energy levels, degeneracy levels, partition functions, and oscillator strengths f_l, which are necessary to calculate the absorption coefficient $\eta_{\rm line}$ of each line in terms of lower (l) and upper (u) level populations n_l and n_u, and their statistical weights g_l and g_u. The absorption coefficient $\eta_{\rm line}$ is given by:

$$\eta_{\rm line} = \frac{\pi e^2}{mc} f_l \frac{n_l}{\rho(r)}\left(1 - \frac{n_u}{n_l}\frac{g_l}{g_u}\right). \quad (9)$$

Elements and ionization stages considered in this work are listed in Table 1.

[6] Atomic data used here are those which were updated by DJH in 2016 (http://kookaburra.phyast.pitt.edu/hillier/cmfgen_files/atomic_data_15nov16.tar.gz).

Table 1
Atomic Elements and Ionization Stages Used to Calculate $\mathcal{M}(t)$

Elem.	Ions	Elem.	Ions
H	I	He	I–II
Li	I–III	Be	I–IV
B	I–V	C	I–IV
N	I–VI	O	I–VI
F	I–VI	Ne	I–VI
Na	I–VI	Mg	I–VI
Al	I–VI	Si	I–VI
P	I–VI	S	I–VI
Cl	I–VI	Ar	I–VI
K	I–VI	Ca	I–VI
Sc	I–VI	Ti	I–VI
V	I–VI	Cr	I–VI
Mn	I–VI	Fe	I–VI
Co	I–VI	Ni	I–VI

3.2. Ionization Equilibrium

Line-acceleration is calculated over the contribution of numerous transitions for every element at every ionization stage present in the wind. Abbott (1982) determined the ionization degrees using the Saha's equation for extended atmospheres (Mihalas 1978), namely:

$$\left(\frac{N_{i+1}}{N_i}\right)_{\rm LTE} = 2\left(\frac{2\pi m_e k_B}{h^2}\right)^{3/2} \frac{T_R\sqrt{T_e}}{N_e/W}\frac{U_{i+1}}{U_i} e^{-\frac{E_i}{k_B T_e}}, \quad (10)$$

where T_R, T_e are the radiation and electron temperatures, respectively, and E_i is the ionization energy from stage i to $i+1$. More precise treatment called *approximate NLTE* (hereafter quasi-NLTE) has been used by, e.g., Mazzali & Lucy (1993) and Noebauer & Sim (2015). Here the ionization balance is determined by the application of the modified nebular approximation (Abbott & Lucy 1985). Following this treatment, the ratio of number densities for two consecutive ions can be expressed in term of its LTE value, multiplied by correction effects due to dilution of radiation field and recombinations:

$$\frac{N_{i+1}}{N_i} \approx \left(\frac{N_e}{W}\right)^{-1} [\zeta_i + W(1-\zeta_i)]\sqrt{\frac{T_e}{T_R}}\left(\frac{N_{i+1}N_e}{N_i}\right)_{\rm LTE}, \quad (11)$$

where ζ_i represents the fraction of recombination processes that go directly to the ground stage. Equation (11) is an alternative description to the one given by Puls et al. (2005), who included a different radiative temperature dependence in the wind, which is especially important in the far-UV region of the spectrum that is not optically thick.

Modifications in the treatment of atomic populations X_i, with i being the excitation level, are also based on the work of Abbott & Lucy (1985). It is necessary to make a distinction between metastable levels (with no permitted electromagnetic dipole transitions to lower energy levels) and all the other ones:

$$\left(\frac{X_i}{X_1}\right) = \begin{cases} \left(\frac{X_i}{X_1}\right)_{\rm LTE} & \text{metastable levels} \\ W(r)\left(\frac{X_i}{X_1}\right)_{\rm LTE} & \text{others.} \end{cases}$$

Atomic partition functions, U_i (necessary for Saha's equation and the calculation of atomic populations), are calculated

following the formulation of Cardona et al. (2010), i.e.,

$$U_i = U_{i,0} + G_{jk} e^{-\varepsilon_{jk}/T} + \frac{m}{3}(n^3 - 343) e^{-\hat{E}_{n*jk}/T}, \quad (12)$$

where $U_{i,0}$ are the constant partition functions, $\hat{E}_{n*jk}$ is the mean excitation energy of the last level of the ion, n is the maximum excitation stage to be considered, while G_{jk}, ε_{jk}, and m are parameters tabulated by Cardona et al. (2010).

The advantage of this treatment is that it provides values for atomic partition functions explicitly as a function of temperature and implicitly of electron density, giving a more accurate ionization balance. Following Noebauer & Sim (2015), the temperature will be treated as a constant ($T_R = T_e = T_{\rm eff}$). Then, for a specific value of ($T_{\rm eff}$, N_e), the ratio between number densities of ionization stages j and i (for a specific Z-element) is calculated by a matrix (hereafter ionization matrix) given by:

$$D_{Z,i,j} = \frac{N_j}{N_i} = \prod_{i \leqslant k < j} \frac{N_{k+1}}{N_k}. \quad (13)$$

In reference to the abundances of the different chemical elements, these were adopted from the solar abundances given by Asplund et al. (2009). However, these can be easily modified to evaluate stars with nonsolar metallicity (see Section 4).

At this point, it is necessary to remark that previous authors (Abbott 1982; Noebauer & Sim 2015) have considered the diluted-electron density N_e/W as constant throughout the wind. Nevertheless, to calculate δ, $\mathcal{M}(t)$ must be evaluated considering changes in the ionization stages, and therefore $N_e(r)/W(r)$. Since, the calculation of electron density depends on the ionization stages of each species which in turn are functions of N_e, we deal with a coupled nonlinear problem. To obtain a solution, we use the following formula to calculate (as an initial value) the electron number density:

$$N_{e,0} = \frac{\rho(r)}{m_{\rm H}} \frac{X_{\rm H} + 2X_{\rm He}}{X_{\rm H} + 4X_{\rm He}}, \quad (14)$$

with $m_{\rm H}$ being the hydrogen atom mass, and $X_{\rm H}$ and $X_{\rm He}$ the abundances of hydrogen and helium, respectively.

We used this initial electron density to start calculating the ionization matrix and to recalculate both atomic populations and electron density iteratively:

$$N_e(r) = \left(X_{\rm H} \frac{D_{1,1,2}}{1 + D_{1,1,2}} + X_{\rm He} \frac{(D_{2,1,2} + 2D_{2,1,3})}{1 + D_{2,1,2} + D_{2,1,3}} \right) \times \frac{\rho(r)}{X_{\rm H} + 4X_{\rm He}}. \quad (15)$$

Convergence of N_e is easily obtained after just a few iterations (see Figure 1). It is important to remark that even when we use $N_{e,0}$ as a constant value (not described by Equation (14)), the final converged value for N_e is the same.

3.3. Radiation Field

Together with an accurate treatment of atomic populations and electron density, Equation (5) requires as an input the radiation field in the term F_ν/F.

Abbott (1982) used the radiation fields from Kurucz' models (Kurucz 1979), whereas Noebauer & Sim (2015) from a blackbody. In this work, we use the radiation field calculated by the NLTE line-blanketing plane-parallel code TLUSTY (Hubeny & Lanz 1995; Lanz & Hubeny 2003).

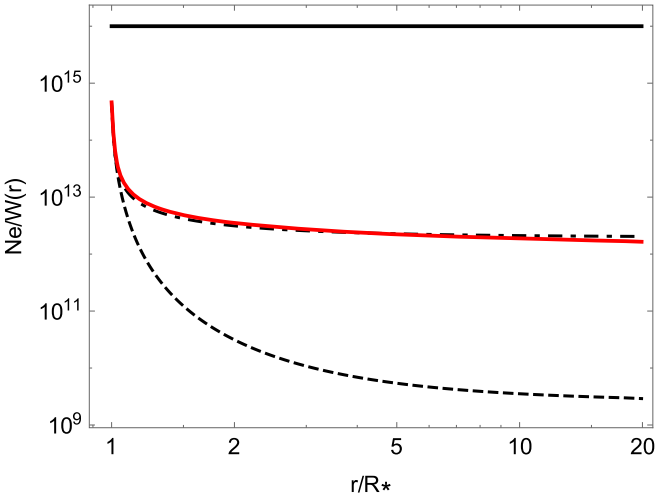

Figure 1. Final value of $N_e/W(r)$ as a function of stellar radius even when $N_{e,0}$ is set as a constant input (black solid line), after one iteration (single dashed line), after two iterations (dashed–dotted line), and after five iterations (red solid line).

The overlap effects among tens of thousands of spectral lines are not considered when we sum the contributions to the force multiplier $\mathcal{M}(t)$ across the wind. However, line-blanketing effects are partially considered as we are using the TLUSTY radiation field in the calculations of $\mathcal{M}(t)$.

3.4. Determination of the Optical Depth Range

Previous studies by Abbott (1982) and Noebauer & Sim (2015) have considered a fixed range for the optical depth t to fit the force multiplier (Equation (8)).

However, given the definition of t (Equation (6)), it is clear that the optical depth range is constrained by the physical properties of the stellar wind (density and velocity profiles). For this reason, calculations presented in this work are constrained inside the wind, characterized by this range of t.

Because m-CAK theory is based upon Sobolev approximation (Sobolev 1960; Lamers & Cassinelli 1999) in this work we will use as upper and lower limits of t its values at the sonic point and at infinity (usually $r \sim 100\,R_*$), respectively. It is important to remark that although t decreases outward it never reaches zero. Therefore, it is always possible to define a proper range.

3.5. Iterative Procedure

Velocity profile and $\dot{M}$ from hydrodynamics is required in order to calculate the line-acceleration $g_{\rm line}$. At the same time, line-force parameters fitted from $g_{\rm line}$, are necessary to solve the m-CAK hydrodynamic equations and obtain the mass-loss rate and velocity profile. Therefore, a self-consistent iterative procedure should be implemented to solve this coupled nonlinear problem.

Our procedure is the following: (i) using a β-law profile with a given mass-loss rate, initial values for the line-force parameters (k_0, α_0, δ_0) are calculated; (ii) a numerical solution of the equation of motion (Equation (3)) is obtained with HYDWIND,[7]

[7] This code solves the m-CAK equation of motion with an eigenvalue that depends on the mass-loss rate. At the location of the singular point, both solution branches (singular point to stellar surface and singular point to infinity) are smoothly merged to obtain the velocity profile, see Pauldrach et al. (1986), Friend & Abbott (1986), and Curé (2004) for details.

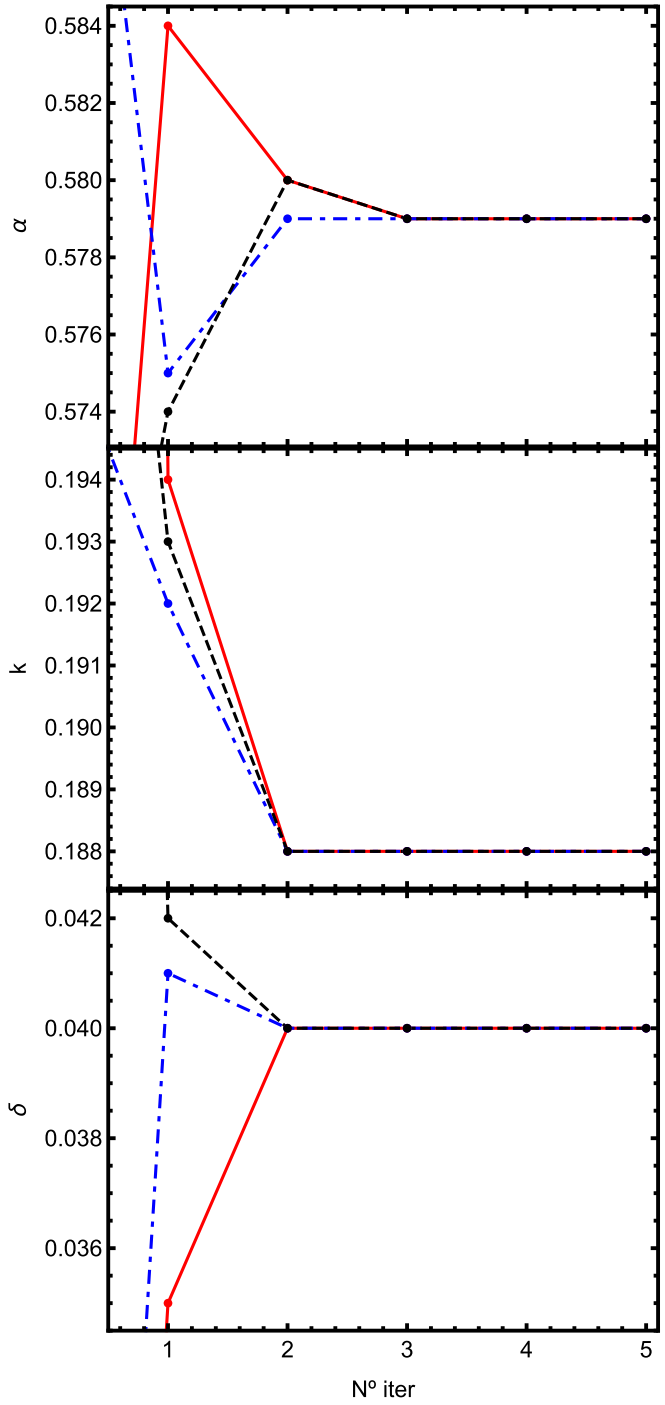

Figure 2. Values of α, k, and δ as a function of the iteration number, starting from different initial values. Different initial values (iteration 0, not shown) converge to the same final self-consistent solution.

getting an improved hydrodynamics: $v(r)$ and $\dot{M}$; (iii) a new force multiplier is calculated; (iv) new line-force parameters (k_i, α_i, δ_i) are fitted from $\mathcal{M}(t)$; and (v) steps ii–iv are iterated. Convergence is usually obtained after ∼4–5 iterations (see Figure 2), independently on the initial values. Our criterion for convergence is when two consecutive iterations (i, $i+1$) get a value for $\|\Delta p\| = \|p^{i+1} - p^i\| \leqslant 10^{-3}$, where p is a line-force parameter and this condition should be satisfied for each one of these parameters.

Figure 3 shows the convergence of the mass-loss rate (top panel) and the terminal velocity (lower panel) as a function of the procedure's iterations. Both values depend nonlinearly on the stellar and line-force parameters.

3.6. A Single-step Test

To compare our line-force parameters with the results obtained by Abbott (1982) and Noebauer & Sim (2015), we use one single-step only. Following these authors, δ and N_e/W are set as input and the optical depth range is fixed between $-6 < \log t < -1$. The selection of a fixed interval of $\log t$ does not require any velocity field structure. Furthermore, we have considered Kurucz' and blackbody fluxes to reproduce Abbott (1982) and Noebauer & Sim (2015) calculations, respectively. Then, starting from a β-law and a $\dot{M}$, we calculate k_1 and α_1 (single-step). These results are shown in Table 2. The coefficients of determination, R-Squared, for α and k (respectively) between previous and our single-iteration results are (i) $R^2_\alpha = 0.87$ and $R^2_k = 0.93$ for $T_{\rm eff} \geqslant 40{,}000$ K; (ii) $R^2_\alpha = 0.4$ and $R^2_k = 0.81$ for $T_{\rm eff} \geqslant 30{,}000$ K. We conclude that our calculations reproduced previous results, now using a modern atomic database and abundances.

4. Results

4.1. Self-consistent Calculations

The following results are computed self-consistently with the methodology detailed in Section 3.

Self-consistent solutions for a grid of models are presented in Table 3. The effective temperature ranges from 32 to 45 kK and $\log g$ from 3.4 to 4.0 dex. This grid considers different stellar radii and two abundances: 1 and 1/5 of the solar value. This table shows the stellar parameters, the calculated t-range, and the fitted m-CAK line-force. In addition, we calculated the corresponding wind solution using HYDWIND, and their error margins were derived considering variations of $\Delta T_{\rm eff} = \pm 500$, $\Delta \log g = \pm 0.05$, and $\Delta R_* = \pm 0.1\, R_\odot$ in the stellar radius, keeping constant the line-force parameters.

Convergence has been checked for each solution. Figure 4 shows the last iteration of $\mathcal{M}(t)$ for four models from Table 3 with different ranges of t. Due to the quasilinear behavior of the logarithm of the force multiplier, parameters k and α are easily fitted and their values can be considered constant throughout the wind (see Section 4.2). To fit δ in the $\mathcal{M}(t)$–N_e/W plane, it is necessary to perform an extra calculation of $\mathcal{M}(t)$ using a slightly different value for the diluted-electron density. Last column of this table shows the ratio between our mass-loss rate and the one calculated using Vink's recipe (Vink et al. 2001), with $v_\infty/v_{\rm esc} = 2.6$ and rescaled to current abundances (Asplund et al. 2009). The mean value of $\dot{M}_{\rm SC}/\dot{M}_{\rm Vink} = 0.98 \pm 0.2$. As we have not included in our procedure multi-line nor line-overlapping processes, we support Puls' (1987) conclusion that these effects are somewhat canceled, because we do not observe relevant discrepancies in the mass-loss rates when a comparison with Vink's recipe is performed.

In Figure 5, we observe clear trends for the behavior of the (k, α, δ) parameters with $T_{\rm eff}$, $\log g$, and Z. While k increases and δ decreases as a function of the effective temperature, for both metallicities. It is interesting to remark the influence of the surface gravity on the resulting line-force parameters, values for k and δ decrease as the gravity decreases. Notice that globally our line-force parameter results are similar to the values obtained in previous works (Puls et al. 2000; Kudritzki 2002; Noebauer & Sim 2015). However, we found

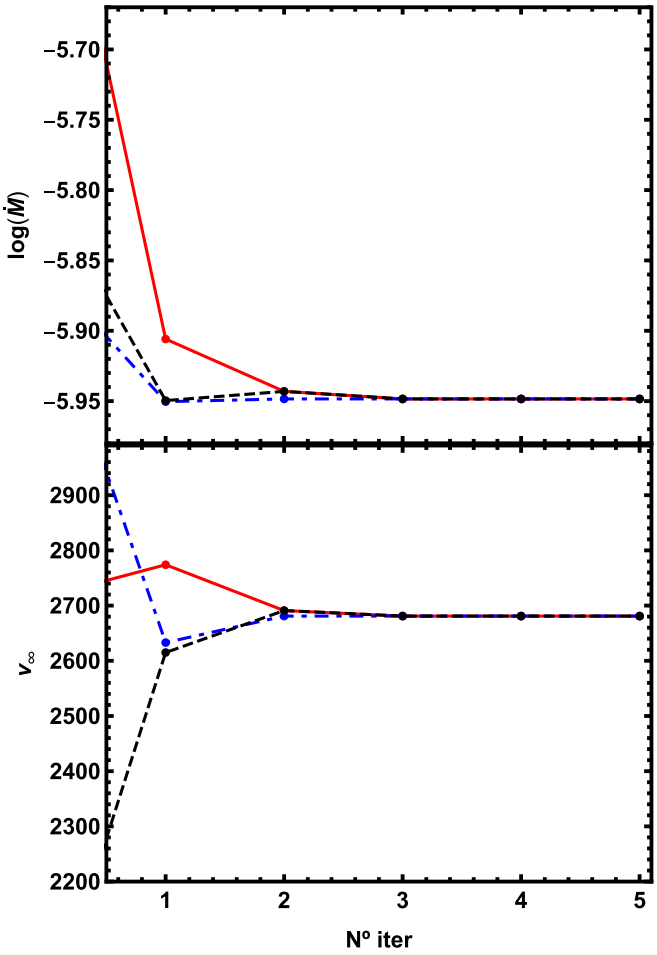

Figure 3. Same as Figure 2, but for the mass-loss rate and terminal velocity.

Table 2
Comparison of k and α Parameters from Abbott (A) and Noebauer & Sim (N), with Our One Single-step Results

				Previous Studies		Present Work	
	$T_{\rm eff}$ (kK)	N_e/W (cm^{-3})	δ	k	α	k_1	α_1
A	30	1.0×10^{8}	0.12	0.093	0.576	0.062	0.661
A	30	1.0×10^{11}	0.12	0.156	0.609	0.097	0.611
A	30	1.0×10^{14}	0.12	0.571	0.545	0.487	0.450
A	40	1.8×10^{8}	0.12	0.051	0.684	0.072	0.639
A	40	1.8×10^{11}	0.12	0.174	0.606	0.120	0.609
A	40	1.8×10^{14}	0.12	0.533	0.571	0.289	0.552
N	42	1.0×10^{15}	0.0	0.381	0.595	0.376	0.572
A	50	3.1×10^{8}	0.092	0.089	0.640	0.148	0.611
A	50	3.1×10^{11}	0.092	0.178	0.606	0.196	0.595
A	50	3.1×10^{14}	0.092	0.472	0.582	0.289	0.566

an important dependence on $\log g$ as a result of the hydrodynamic coupling in the self-consistent procedure.

On the other hand, the behavior of α depends on the metallicity, it increases with effective temperature for solar abundance, but for low abundance and low gravities, it slowly decreases with temperature. Moreover, the change in α is more significant for $\log g$ than for $T_{\rm eff}$: a difference in $\Delta \log g \pm 0.2$ dex produces a $\Delta\alpha \sim 0.04$, whereas variations on $\Delta T_{\rm eff} = \pm 2000$ K, might produce $\Delta\alpha \sim 0.02$.

Figure 6 shows the results for the mass-loss rates as a function of the effective temperature, for different gravities and metallicities. The upper panel shows the results from our self-consistent procedure and the bottom panel shows the result using Abbott's methodology (a single iteration) to calculate line-force parameters and apply them in our hydrodynamic code HYDWIND (hereafter Abbott's procedure). We found that $\dot{M}$ increases with effective temperature and metallicity and decreases with gravity. This behavior is similar to the one obtained using Abbott's procedure, but the self-consistent calculated mass-loss rates are about 30% larger.

From the mass-loss results tabulated in Table 3, a simple relationship for solar-like metallicities (with a coefficient of determination or R-squared, $R^2 = 0.999$) reads:

$$\begin{aligned}\log \dot{M}_{Z=1.0} = {} & 10.443 \times \log\left(\frac{T_{\rm eff}}{1000\ {\rm K}}\right) \\ & - 1.96 \times \log g \\ & + 0.0314 \times (R_*/R_\odot) \\ & - 15.49, \end{aligned} \quad (16)$$

and for metallicity $Z/Z_\odot = 0.2$ the relationship reads (with $R^2 = 0.999$):

$$\begin{aligned}\log \dot{M}_{Z=0.2} = {} & 11.668 \times \log\left(\frac{T_{\rm eff}}{1000\ {\rm K}}\right) \\ & - 2.126 \times \log g \\ & + 0.04 \times (R_*/R_\odot) \\ & - 17.63, \end{aligned} \quad (17)$$

where $\dot{M}$ is given in $10^{-6}\, M_\odot\ {\rm yr}^{-1}$. These relationships could be considered analogous to that given by Vink et al. (2000) to obtain theoretical mass-loss rates for solar-like metallicities. However, the advantage of our description is that it depends only on *stellar parameters* and we do not need to consider the value of $v_\infty/v_{\rm esc}$. It is important to remark, however, that this formula has been derived for the following ranges:

1. $T_{\rm eff} = 32$–45 kK
2. $\log g = 3.4$–4.25
3. $M_*/M_\odot \geqslant 25.0$.

Concerning terminal velocities, see Figure 7, self-consistent calculations (top panel) show that v_∞ is almost constant with respect to the effective temperature, but it decreases as a function of $\log g$ and Z. On the other hand, Abbott's procedure results do not show the same behavior and exhibit a maximum in the $T_{\rm eff}$ interval.

4.2. Range of Validity for Line-force Parameters

It is important to remember that the range of optical depths used to calculate our self-consistent line-force parameters is defined along almost all the atmosphere of the star, i.e., downstream from the sonic point. This procedure improves the criterion used by Abbott (1982), who determined the parameters at $t = 10^{-4}$. This value sometimes lays outside the optical depth range here defined, as shown in Figure 4.

To analyze the change on the line-force parameters due to the selection of the t-range, we define four different intervals inside the whole range of t, and compute these parameters in each range. Table 4 summarizes these calculations. Regarding the uncertainties of our procedure in the terminal velocities,

Table 3
Self-consistent Line-force Parameters (k, α, δ) for Adopted Standard Stellar Parameters, Together with the Resulting Terminal Velocities and Mass-loss Rates ($\dot{M}_{\rm SC}$)

$T_{\rm eff}$ (kK)	$\log g$	$R_*/R_\odot$	$Z/Z_\odot$	$\log t_{\rm in}$	$\log t_{\rm out}$	k	α	δ	$v_\infty^{\rm SC}$ (km s^{-1})	$\dot{M}_{\rm SC}$ ($10^{-6}\,M_\odot$ yr^{-1})	$\dot{M}_{\rm SC}/\dot{M}_{\rm Vink}$
45	4.0	12.0	1.0	−0.31	−4.53	0.167	0.600	0.021	3 432 ± 240	$2.0\pm^{0.65}_{0.5}$	1.00
45	4.0	12.0	0.2	−0.77	−4.85	0.142	0.493	0.017	2 329 ± 210	$0.38\pm^{0.15}_{0.11}$	0.74
45	3.8	16.0	1.0	0.28	−4.07	0.135	0.648	0.022	3 250 ± 300	$6.4\pm^{1.6}_{1.3}$	0.84
45	3.8	16.0	0.2	−0.06	−4.28	0.114	0.545	0.014	2 221 ± 230	$1.7\pm^{0.6}_{0.45}$	0.88
42	3.8	16.0	1.0	−0.10	−4.36	0.137	0.629	0.027	3 235 ± 300	$3.4\pm^{0.9}_{0.7}$	0.94
42	3.8	16.0	0.2	−0.55	−4.73	0.108	0.534	0.019	2 313 ± 230	$0.73\pm^{0.3}_{0.21}$	0.79
42	3.6	20.4	1.0	0.70	−3.80	0.122	0.671	0.039	2 738 ± 230	$11\pm^{3.5}_{2.5}$	0.74
42	3.6	20.4	0.2	0.37	−4.09	0.091	0.586	0.022	2 043 ± 200	$3.1\pm^{1.2}_{0.75}$	0.82
40	4.0	12.0	1.0	−0.88	−4.97	0.164	0.581	0.027	3 300 ± 220	$0.66\pm^{0.19}_{0.15}$	1.17
40	4.0	12.0	0.2	−1.43	−5.44	0.133	0.492	0.038	2 329 ± 160	$0.11\pm^{0.05}_{0.03}$	0.76
40	3.6	20.4	1.0	0.42	−3.96	0.118	0.659	0.044	2 813 ± 290	$6.6\pm^{1.8}_{1.4}$	0.89
40	3.6	20.4	0.2	−0.05	−4.40	0.091	0.572	0.025	2 116 ± 230	$1.7\pm^{0.5}_{0.4}$	0.90
40	3.4	18.0	1.0	1.30	−3.14	0.099	0.715	0.094	1 548 ± 240	$14.5\pm^{5.0}_{3.5}$	0.73
40	3.4	18.0	0.2	1.90	−3.50	0.073	0.650	0.047	1 334 ± 230	$4.7\pm^{2.4}_{1.3}$	0.92
38	3.8	16.0	1.0	−0.63	−4.79	0.130	0.610	0.036	3 153 ± 240	$1.2\pm^{0.3}_{0.25}$	1.10
38	3.8	16.0	0.2	−1.18	−5.28	0.091	0.542	0.033	2 473 ± 300	$0.25\pm^{0.08}_{0.06}$	0.89
36	4.0	12.0	1.0	−1.45	−5.50	0.132	0.580	0.036	3 314 ± 200	$0.21\pm^{0.065}_{0.05}$	1.17
36	4.0	12.0	0.2	−1.97	−5.97	0.101	0.517	0.068	2 402 ± 140	$0.036\pm^{0.014}_{0.01}$	0.78
36	3.6	20.4	1.0	−0.29	−4.55	0.104	0.644	0.062	2 809 ± 240	$2.2\pm^{0.7}_{0.5}$	1.12
36	3.6	20.4	0.2	−0.87	−5.09	0.071	0.581	0.033	2 534 ± 220	$0.5\pm^{0.17}_{0.13}$	1.00
36	3.4	18.0	1.0	1.78	−3.77	0.091	0.686	0.116	1 708 ± 170	$4.4\pm^{1.6}_{1.0}$	1.13
36	3.4	18.0	0.2	0.41	−4.21	0.072	0.607	0.048	1 566 ± 160	$1.0\pm^{0.4}_{0.25}$	1.01
34	3.8	16.0	1.0	−1.27	−5.37	0.103	0.604	0.043	3 093 ± 210	$0.34\pm^{0.1}_{0.07}$	1.12
34	3.8	16.0	0.2	−1.93	−5.94	0.069	0.555	0.028	2 791 ± 180	$0.074\pm^{0.025}_{0.018}$	0.95
34	3.6	20.4	1.0	−0.61	−4.82	0.095	0.637	0.074	2 732 ± 180	$1.2\pm^{0.4}_{0.3}$	1.25
34	3.6	20.4	0.2	−1.29	−5.46	0.058	0.590	0.031	2 642 ± 180	$0.25\pm^{0.07}_{0.05}$	1.03
32	3.4	18.0	1.0	0.37	−4.30	0.078	0.675	0.159	1 653 ± 190	$1.3\pm^{0.5}_{0.3}$	1.67
32	3.4	18.0	0.2	−0.70	−4.15	0.053	0.610	0.052	1 847 ± 140	$0.23\pm^{0.075}_{0.05}$	1.16

Note. Ratios between self-consistent mass-loss rates and Vink's recipe values (rescaled to match metallicity from Asplund et al. 2009) using $v_\infty/v_{\rm esc} = 2.6$ are shown in the last column. Error margins for mass-loss rates and terminal velocities are derived over a variation of ±500 for effective temperature, ±0.05 for logarithm of surface gravity, and ±0.1 for stellar radius.

these are of the same order as the uncertainties owed to the errors in the determination of the stellar parameters in the range 32,000 K $< T_{\rm eff} <$ 40,000 K, while, the uncertainties in $\dot{M}$ are much lower than the ones produced by variations of stellar parameters. These small uncertainties indicate that it is a good approximation to consider line-force parameters as constants throughout the wind. Due to the fact that the entire t-range represents the physical conditions of almost all the wind, we recommend using the complete optical depth range to derive the line-force parameters.

For $T_{\rm eff} <$ 30,000 K, we found that $\log \mathcal{M}(t)$ is no longer linear with respect to $\log t$ and the corresponding line-force parameters can be approximated to a linear piecewise description. Due to this reason, we establish that our set of self-consistent solutions describes stellar winds for effective temperatures and $\log g$ in the range 32,000–45,000 K and 3.4–4.0 dex, respectively.

5. Synthetic Spectra

In order to know whether our calculations reproduce realistic physical features observed in hot stars, we calculate synthetic spectra for three O-type stars using FASTWIND. We select some stars in the range of the considered $T_{\rm eff}$, trying to cover the extreme cases of temperature and $\log g$. We choose first the O4 I(n)fp star ζ-Puppis (HD 66811) because it has been extensively studied (Puls et al. 1996, 2006; Repolust et al. 2004; Sota et al. 2011; Bouret et al. 2012; Noebauer & Sim 2015). Mentioned authors have independently adopted different sets of stellar and wind parameters, which are summarized in Table 5. Here, the wind parameters were determined by Repolust et al. (2004). Puls et al. (2006) has used their parameters and derived clumped mass-loss rates from Hα, IR, and radio, using analytical expressions for the corresponding opacities, whereas Bouret et al. (2012) used CMFGEN. Both calculations include clumping, so these results correspond to a clumped mass-loss rate.[8] On the other hand, the mass-loss rate given by Noebauer & Sim (2015) was obtained using their Monte-Carlo radiation hydrodynamics (MCRH) method assuming a homogeneous media ($f_{\rm cl} = 1.0$).

Particularly, we compare our results with those given by Puls et al. (2006), who did an exhaustive analysis of the clumping throughout the wind. Two different values for mass-loss rate are given by these authors, because they considered different

[8] FASTWIND uses the clumping factor $f_{\rm cl} \geqslant 1$ (with $f_{\rm cl} = 1$ representing the smooth limit), where $f_{\rm cl} = 1/f$ if the inter-clump medium was void (Sundqvist & Puls 2018). On the other hand, CMFGEN-clumping is represented by the so-called volume filling factor f, which scales homogeneous and clumped mass-loss rates under the relationship $\dot{M}_{\rm hom} = \dot{M}_{\rm clump}/\sqrt{f}$ (notice that this f takes values between 0 and 1).

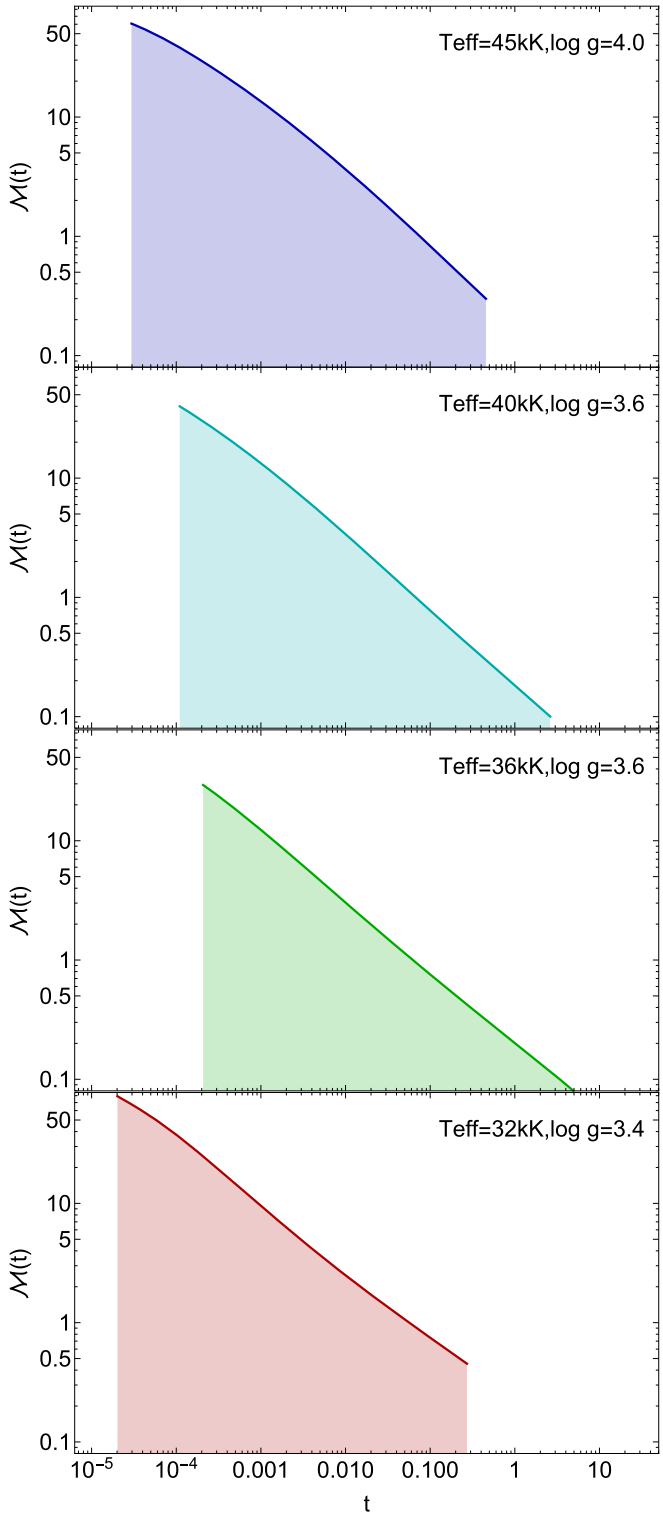

Figure 4. Force multiplier $\mathcal{M}(t)$ as function of t for some stellar models presented on Table 3 with $T_{\rm eff} = 45{,}000$ K and $\log g = 4.0$ (blue), $T_{\rm eff} = 40{,}000$ K and $\log g = 3.6$ (cyan), $T_{\rm eff} = 36{,}000$ K and $\log g = 3.4$ (green), and $T_{\rm eff} = 32{,}000$ K and $\log g = 3.4$ (red). Colored areas below curves indicate the range of t, where the fits for (k, α, δ) have been adjusted.

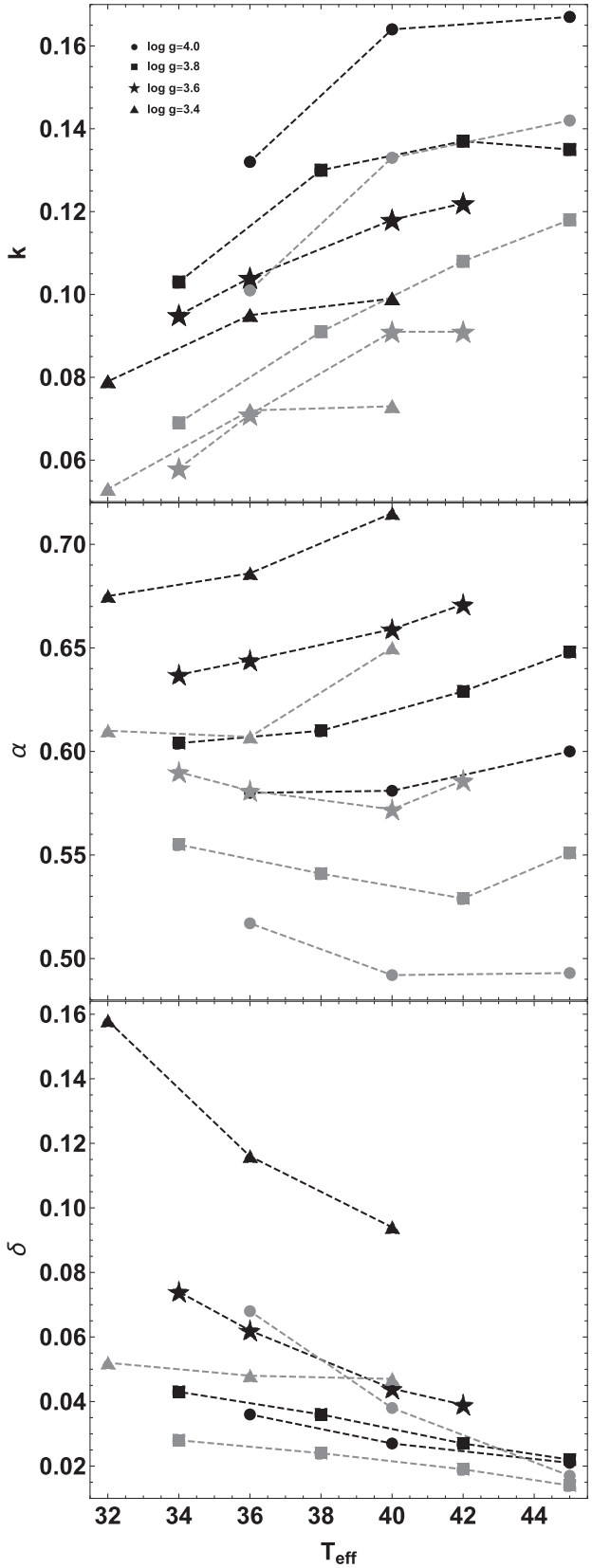

Figure 5. Behavior of line-force parameters (k, α, δ) as a function of the effective temperature (in kK), for different surface gravities and metallicities. Circles represent models with $\log g = 4.0$, squares: $\log g = 3.8$, stars: $\log g = 3.6$, and triangles: $\log g = 3.4$. Black dashed lines are for models with solar metallicity and gray dashed lines for $Z = Z_{\odot}/5$.

stellar radii depending on the assumed distance for ζ-Puppis: (i) the "conventional" ($d = 460$ pc) and (ii) the one given by Sahu & Blaauw (1993, $d = 730$ pc). We examine here the

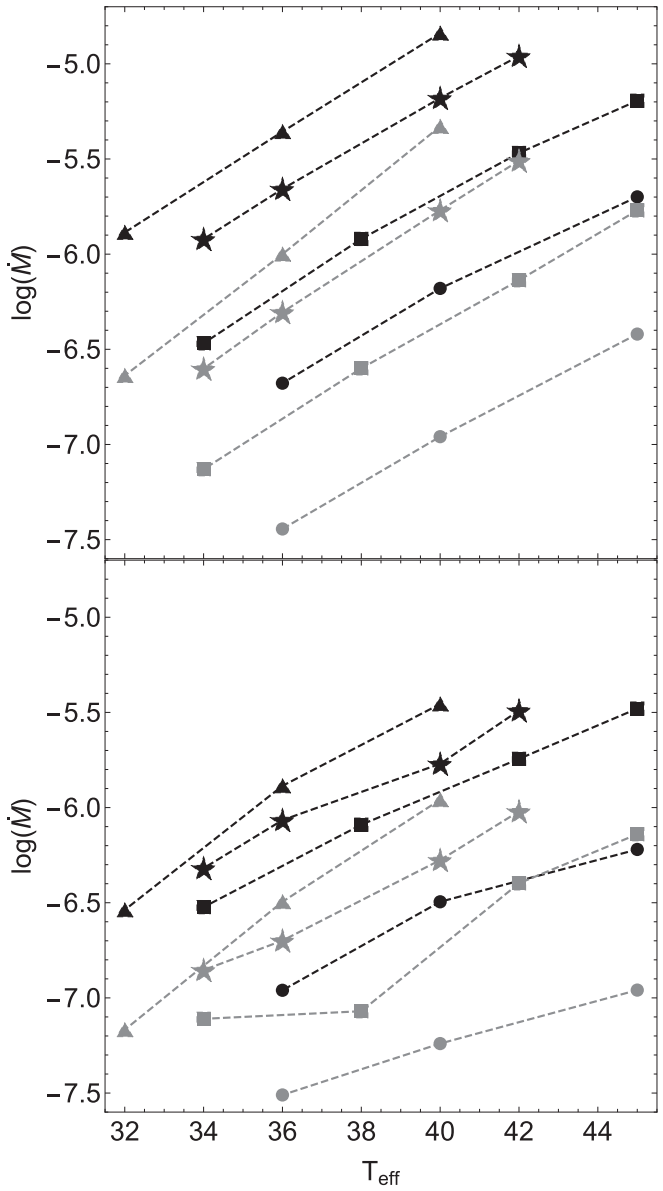

Figure 6. Behavior of mass-loss rate as a function of effective temperature (in kK) for different abundances and gravities. Top panel is for self-consistent calculations and bottom panel is for Abbott's procedure, now including the finite-disk correction factor. Symbol description is the same as that in Figure 5.

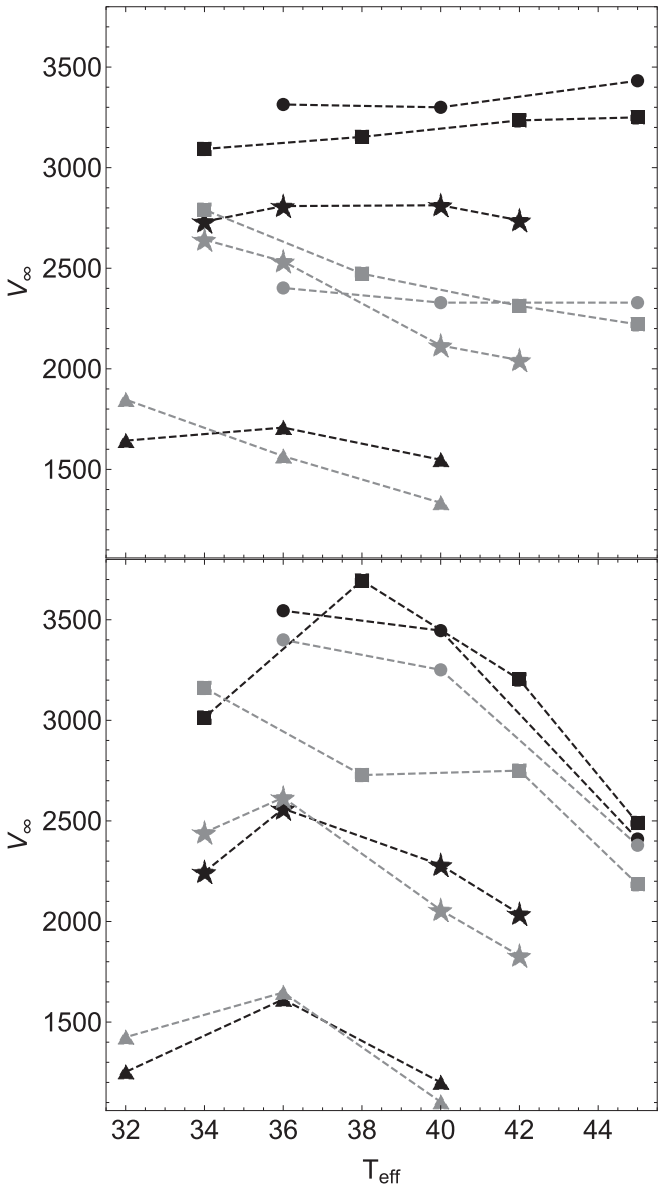

Figure 7. Same as Figure 6, but for the terminal velocities.

"conventional" case with $R_*/R_\odot = 18.6$. We can observe from Table 5 (last row), that our new calculated mass-loss rate agree quite well with the value from Puls et al. (2006).

Figure 8 shows the observed spectra (kindly provided by D. J. Hillier) and the resulting synthetic spectra for ζ-Puppis. Stellar parameters are taken from Puls et al. (2006, see Table 5) and wind parameters from our self-consistent procedure ($\dot{M}_{SC} = 4.6 \times 10^{-6}\, M_\odot\ \mathrm{yr}^{-1}$). We calculated three synthetic spectra with different clumping factors: $f_{cl} = 1.0$ (homogeneous), $f_{cl} = 5.0$, and $f_{cl} = 9.0$. The best fit is for $f_{cl} = 5.0$, which is the same clumping factor found by Puls et al. (2006) with their $\dot{M} = 4.2 \times 10^{-6}\, M_\odot\,\mathrm{yr}^{-1}$. Moreover, we also include the synthetic spectra obtained with the self-consistent solution (see Figure 9), calculated using the stellar parameters given by Bouret et al. (2012, see Table 5) and Najarro et al. (2011). The best fit is achieved when we use a clumping factor of $f_{cl} = 5.0$. These results suggest that the real stellar parameters lie in the neighborhood given by Puls et al. (2006) and Najarro et al. (2011).

The observed spectrum for HD 163758 (O9 I) has been obtained from the UVES-POP database.[9] We calculated the synthetic spectra for this star (see Figure 10) using stellar parameters from Bouret et al. (2012) and wind self-consistent parameters (see Table 6) with different clumping factors, the best fit is for $f_{cl} = 6.0$.

Last spectrum corresponds to the O3.5 V star HD 164794, also obtained from the UVES-POP database. Stellar parameters were extracted from Krtička et al. (2015), as shown in Table 6. Contrary to previous cases, the best fit is obtained for the homogeneous model ($f_{cl} = 1.0$, see Figure 11).

In view of these first results, our self-consistent iterative procedure takes us quickly into the neighborhood of the solution that reproduces the observed wind spectra for O-type stars.

[9] http://www.eso.org/sci/observing/tools/uvespop/field_stars_uptonow.html

Table 4
Influence of the Optical Depth Interval on the Line-force Parameters for Some Reference Models Given in Table 3

$T_{\rm eff}$	$\log g$	$\log t_{\rm in}$	$\log t_{\rm out}$	k	α	δ	$\lvert\Delta v_\infty\rvert$ (km s^{-1})	$\lvert\Delta \dot{M}\rvert$ ($10^{-6}\,M_\odot$ yr^{-1})
45,000	4.0	−0.31	−2.03	0.099	0.686	0.037	780	0.23
		−0.31	−2.87	0.107	0.650	0.029	600	0.30
		−0.31	−3.71	0.120	0.638	0.027	420	0.21
		−0.31	−4.55	0.167	0.600	0.021	0	0
40,000	4.0	−0.87	−2.50	0.099	0.633	0.040	521	0.09
		−0.87	−3.32	0.099	0.634	0.036	610	0.07
		−0.87	−4.14	0.107	0.621	0.026	594	0.07
		−0.87	−4.96	0.164	0.581	0.027	0	0
40,000	3.6	0.08	−1.44	0.095	0.666	0.090	247	0.58
		0.08	−2.28	0.098	0.680	0.075	75	0.13
		0.08	−3.12	0.101	0.692	0.067	323	0.92
		0.08	−3.96	0.118	0.659	0.044	0	0
36,000	3.6	−0.29	−2.00	0.084	0.637	0.112	520	0.58
		−0.29	−2.85	0.092	0.648	0.078	114	0.15
		−0.29	−3.70	0.089	0.668	0.075	267	0.01
		−0.29	−4.55	0.104	0.644	0.062	0	0
32,000	3.4	0.37	−1.49	0.066	0.630	0.251	631	0.77
		0.37	−2.43	0.075	0.636	0.221	457	0.57
		0.37	−3.37	0.079	0.662	0.179	168	0.11
		0.37	−4.31	0.078	0.675	0.159	0	0

Note. Absolute values of the differences in the resulting Wind parameters with respect to the reference solution are presented.

Table 5
Stellar and Wind Parameters for ζ-Puppis from Previous Studies Compared with Our Self-consistent Results

Previous Studies						Present Work				
Reference	$T_{\rm eff}$ (kK)	$\log g$	$R_*/R_\odot$	$\dot{M}$ ($10^{-6}\,M_\odot$ yr^{-1})	v_∞ (km s^{-1})	k	α	δ	$\dot{M}_{\rm SC}$ ($10^{-6}\,M_\odot$ yr^{-1})	$v_\infty^{\rm SC}$ (km s^{-1})
Noebauer & Sim (2015)	42	3.6	19.0	45.0	881	0.120	0.678	0.041	$11.0\pm^{3.5}_{3.0}$	2 500 ± 280
Bouret et al. (2012)	40	3.64	18.7	2.0	2300	0.120	0.655	0.039	$5.2\pm^{1.6}_{1.2}$	2 700 ± 300
Puls et al. (2006)	39	3.6	29.7	8.5	2250	0.115	0.654	0.044	$9.3\pm^{2.9}_{2.2}$	3200 ± 350
	39	3.6	18.6	4.2	2250	0.114	0.658	0.049	$4.6\pm^{1.3}_{1.1}$	2 570 ± 300

Note. Line-force parameters are also listed.

6. Discussion

We have developed a self-consistent methodology to calculate the line-force parameters and derived consequently mass-loss rates and velocity profiles. We found that mass-loss rate is about 30% larger than the one obtained using Abbott's procedure (non-self-consistent calculation).

6.1. Terminal Velocity

It is well known that the scaling relation for the terminal velocity in the frame of the line-driven wind theory. This relation (Puls et al. 2008) reads:

$$v_\infty \approx 2.25\sqrt{\frac{\alpha}{1-\alpha}}\,v_{\rm esc}. \quad (18)$$

This is an approximation of the formula found by Kudritzki et al. (1989, their Equations (62) to (65)).

In Figure 12 we have plotted $v_\infty/v_{\rm esc}$ versus $\sqrt{\alpha/(1-\alpha)}$ using the results from Table 3. Contrary to the expected result (Equation (18)) for solar abundances, we find a different linear behavior that strongly depends on the value of $\log g$. This is a new result that comes from applying our self-consistent procedure. The m-CAK equation of motion shows an interplay between the gravity ($\log g$) and the line-force term. This balance of forces defines the location of the singular point and therefore fixes the value of $\dot{M}$. As a consequence, the velocity profile depends also on the value of $\log g$. This result cannot be obtained from Equation (18) which is an oversimplification of this nonlinear coupling. However, Equation (18) presents a fair fit when $Z = Z_\odot/5$, where the dependence of the slope on $\log g$ is weak because the radiation force is driven by fewer ions.

The dependence of $v_\infty/v_{\rm esc}$ on $\log g$ yield that stars with solar abundances present an intrinsic variations of $v_\infty/v_{\rm esc}$ in the range of 2.4–3.7, as shown in Figure 12. This range might explain the scatter observed on the hot side of the bistability jump shown by Markova & Puls (2008, in their Figure 12).

6.2. Mass-loss Rate

In this section we want to compare our theoretical results with the ones obtained from line-profile fittings for homogeneous (unclumped) winds with a β-law, and the mass-loss (recipe) from Vink et al. (2000).

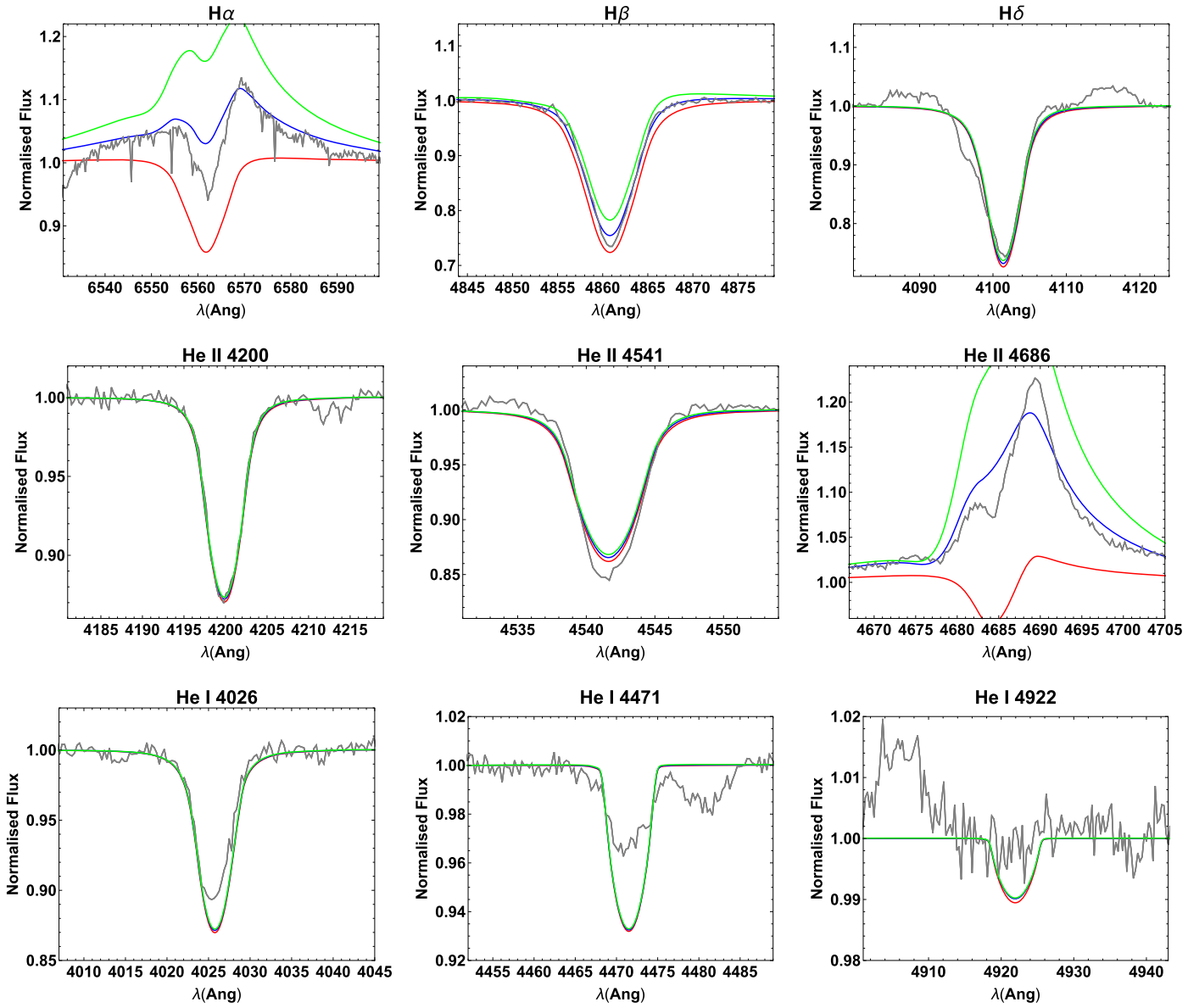

Figure 8. Resulting FASTWIND spectra for ζ-Puppis with $T_{\rm eff} = 39$ kK, $\log g = 3.6$, $R_*/R_\odot = 18.6$, and $\dot{M} = 4.6 \times 10^{-6}\ M_\odot\ {\rm yr}^{-1}$. Clumping factors are $f_{\rm cl} = 1.0$ (red, homogeneous), $f_{\rm cl} = 5.0$ (blue), and $f_{\rm cl} = 9.0$ (green).

Table 6
Same As Table 5, but for HD 163758 and HD 164794

Previous Studies						Present Work				
Name	$T_{\rm eff}$ (kK)	$\log g$	$R_*/R_\odot$	$\dot{M}$ ($10^{-6}\ M_\odot\ {\rm yr}^{-1}$)	v_∞ (km s^{-1})	k	α	δ	$\dot{M}_{\rm SC}$ ($10^{-6}\ M_\odot\ {\rm yr}^{-1}$)	$v_\infty^{\rm SC}$ (km s^{-1})
HD 163758	34.5	3.41	21.0	1.6	2100	0.087	0.679	0.112	$3.3 \pm {}^{1.1}_{0.8}$	2040 ± 280
HD 164794	43.8	3.92	13.1	2.9	3090	0.141	0.614	0.020	$2.3 \pm {}^{0.6}_{0.5}$	$3\,304 \pm 400$

Note. Stellar and wind parameters are from Bouret et al. (2012) and Krtička et al. (2015) respectively.

Table 7 shows our results for the only two O-type star reported by Bouret et al. (2005): HD 96715, $T_{\rm eff} = 43.5$ kK, $\log g = 4.0$, and HD 1904290A, $T_{\rm eff} = 39$ kK, $\log g = 3.6$. These results were obtained for the self-consistent solution together with the ones after just one iteration starting from a β-law. It is observed that models starting from a β-law largely overestimate the terminal velocity and slightly underestimate the mass-loss rate. Self-consistent calculations find a fairly good agreement to both: the observed mass-loss rate and terminal velocity. For the mass-loss rate in this figure, we have included the result calculated using Vink et al.'s (2000) recipe. It is clear that our self-consistent method gives values of $\dot{M}$ much closer to the observed ones.

We also apply our self-consistent procedure to objects analyzed by means of FASTWIND adopting unclumped winds.

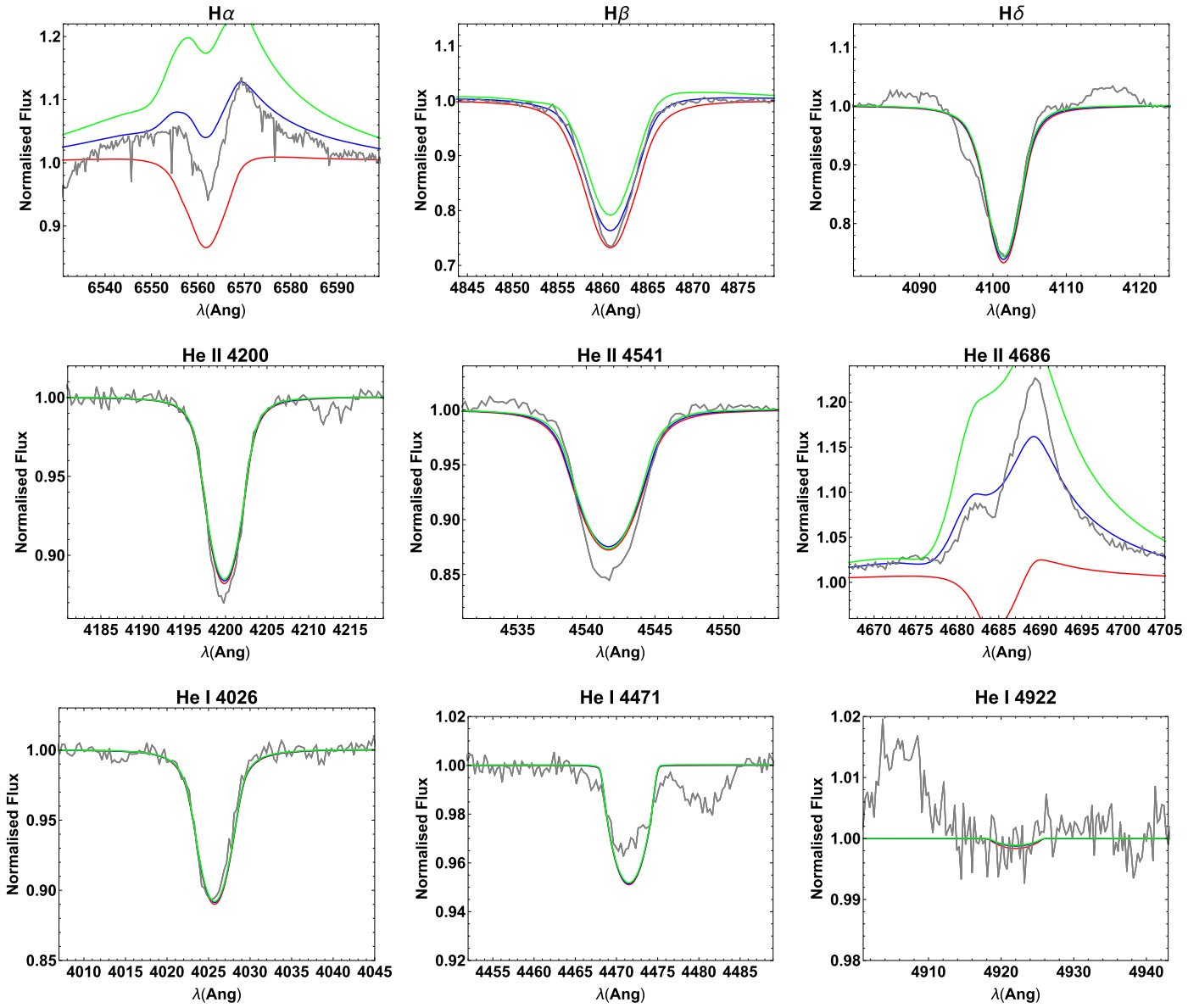

Figure 9. Resulting FASTWIND spectra for ζ-Puppis with $T_{\rm eff} = 40$ kK, $\log g = 3.64$, $R_*/R_\odot = 18.6$, and $\dot{M} = 5.2 \times 10^{-6}\, M_\odot\, {\rm yr}^{-1}$. Clumping factors are $f_{\rm cl} = 1.0$ (red, homogeneous), $f_{\rm cl} = 5.0$ (blue), and $f_{\rm cl} = 9.0$ (green).

Table 7
Comparison of Self-consistent with β-law (Single-step) Models for the Two Stars Analyzed By Bouret et al. (2005)

Model	$T_{\rm eff}$ (kK)	$\log g$	$R_*/R_\odot$	k	α	δ	v_∞ (km s^{-1})	$\dot{M}$ ($10^{-6}\, M_\odot\, {\rm yr}^{-1}$)
Self-Consistent	43.5	4.0	11.9	0.159	0.603	0.032	3 342 ± 240	$1.55\pm^{0.45}_{0.3}$
$\beta = 1.0$	43.5	4.0	11.9	0.118	0.647	0.021	4 187 ± 290	$1.45\pm^{0.35}_{0.25}$
Self-Consistent	39	3.6	19.45	0.116	0.657	0.079	2 412 ± 210	$5.8\pm^{2.0}_{1.3}$
$\beta = 0.8$	39	3.6	19.45	0.039	0.815	0.062	6 789 ± 570	$4.2\pm^{0.9}_{0.7}$

Note. Self-consistent models reproduce better the line-fitted Wind parameters obtained by these authors ($\beta = 1$: $v_\infty = 3000$ km s^{-1}, $\dot{M} = 1.8 \times 10^{-6}\, M_\odot\, {\rm yr}^{-1}$, and $\beta = 0.8$: $v_\infty = 2300$ km s^{-1}, $\dot{M} = 6 \times 10^{-6}\, M_\odot\, {\rm yr}^{-1}$).

For that purpose, we also examine some field Galactic O-type stars from Markova et al. (2018). Table 8 summarizes our results. We found a fair agreement between observed and calculated mass-loss rates (see Figure 13). These results confirm that our methodology delivers the proper mass-loss rate for the ranges in $T_{\rm eff}$ and $\log g$ given above. Below these thresholds, mass-loss rates present larger values compared with both: observational and Vink's theoretical values. This is probably due to the fact that the line-force multiplier is no longer a linear function of t (in the log-log plane, see Figure 4), and the line-force parameters are not constant throughout the wind.

Table 8
Resulting Self-consistent Wind Parameters (v_∞^{SC} and $\dot{M}_{SC}$) Calculated for Stars Analyzed by Markova et al. (2018)

Field Star	T_{eff} (kK)	log g	$R_*/R_\odot$	k	α	δ	v_∞^{SC} (km s^{-1})	$\dot{M}$ (10^{-6} $M_\odot$ yr^{-1})	$\dot{M}_{SC}/\dot{M}_{obs}$	$\dot{M}_{SC}/\dot{M}_{Vink}$
HD 169582	37	3.5	27.2	0.102	0.668	0.063	3017 ± 700	$7.1\pm^{3.6}_{2.4}$	1.10	1.26
CD-43 4690	37	3.61	14.1	0.105	0.653	0.058	2 310 ± 540	$1.5\pm^{0.9}_{0.55}$	1.22	1.16
HD 97848	36.5	3.9	8.2	0.123	0.601	0.034	2532 ± 470	$0.17\pm^{0.09}_{0.06}$	0.89	0.95
HD 69464	36	3.51	20.0	0.099	0.664	0.076	2412 ± 580	$3.2\pm^{1.9}_{1.2}$	1.14	1.30
HD 302505	34	3.6	14.1	0.092	0.643	0.077	2331 ± 460	$0.68\pm^{0.42}_{0.26}$	1.24	0.98
HD 148546	31	3.22	24.4	0.073	0.718	0.243	1300 ± 350	$5.3\pm^{4.7}_{2.5}$	0.94	2.24
HD 76968a	31	3.25	21.3	0.071	0.711	0.248	1212 ± 300	$3.5\pm^{3.3}_{1.7}$	1.43	2.11
HD 69106	30	3.55	14.2	0.068	0.644	0.149	1455 ± 300	$0.21\pm^{0.16}_{0.09}$	1.48	1.78

Note. Error margins presented here for Wind parameters are undergone from uncertainties of ±1000 for T_{eff} and ±0.1 for log g. The last two columns show the ratio between self-consistent and observed mass-loss rates and the ratio between self-consistent and Vink's mass-loss rates.

However, it is important to remark that uncertainties of $\Delta T_{eff} \sim \pm 1000$ K and $\Delta \log g \sim \pm 0.1$ dex, produce uncertainties in the mass-loss rates up to a factor of 2 (see blue error bar in the top panel of Figure 13), which can be considered as the upper threshold for the mass-loss rate. Hence, even though our self-consistent hydrodynamics gives confident values for $\dot{M}$, these good results are strongly dependent on the assumed stellar parameters.

7. Conclusions

In the present work we have presented a treatment to calculate self-consistent line-force parameters coupled with the hydrodynamics in the frame of the radiation driven wind theory. Thanks to this procedure, we achieve a unique well-converged solution that does not depend on the chosen initial values. This is important because it reduces the number of free parameters (now β, v_∞, and $\dot{M}$ are no more input parameters) to be determined by fitting synthetic spectra against observed ones.

Our calculations contemplate the contribution to the line-force multiplier from more than ∼900,000 atomic transitions, an NLTE radiation flux from the photosphere and a quasi-LTE approximation for the occupational numbers. We have to notice that for $T_{eff} > 30{,}000$ K the line-force parameters can be confidently used as constants throughout the wind.

The set of solutions given in Table 3 differs from previous line-force parameter calculations performed by Abbott (1982) and Noebauer & Sim (2015). With these new values, we found a different scale relation for the terminal velocity that is steeper than the usually accepted one. This new relation might explain the observed scatter found in the terminal velocity from massive stars located at the hot side of the bistability jump (Markova & Puls 2008).

Concerning the wind parameters derived from modeling O-type stars with homogeneous winds, our mass-loss rates are in better agreement with the predicted ones given by the Vink et al. (2000) formula.

For the calculation of synthetic spectra for O-type stars (ζ-Puppis, HD 163758, and HD 164794), we conclude that our procedure's values for mass-loss rate and hydrodynamics reproduce the observed line profiles when an adequate value for the clumping factor is chosen.

Even knowing the limitations of the m-CAK theory, this remains an extremely useful framework to get an approach about the real parameters of stellar winds on massive stars. In spite of the approximations assumed under this theory, we obtain reliable values for mass-loss rates and self-consistent hydrodynamics in a short period of time with a great CPU time savings (compare with big efforts made by, e.g., Mokiem et al. 2005 or Fierro-Santillán et al. 2018).

Our new self-consistent procedure can be used to derive accurate mass-loss rates and (i) study evolutionary tracks, where a high precision on terminal velocities is not required, and (ii) derive trusty clumping factors via line-profile fittings.

We sincerely thank J. Puls for helpful discussions that improved this work and for having put at our disposal his code FASTWIND. We thank the anonymous referee for useful comments. We are very grateful to D. J. Hillier for allowing us to use CMFGEN-atomic-data and providing us with the observed spectrum of ζ-Puppis. We also thank C. Arcos for her help with the code TLUSTY. A.C.G.M. has been financially supported by the PhD Scholarship folio N° 2116 1426 from National Commission for Scientific and Technological Research of Chile (CONICYT). A.C.G.M. is also thankful for support from the Chilean Astronomical Society (SOCHIAS). A.C.G.M. and M.C. acknowledge support from Centro de Astrofísica de Valparaíso. M.C. thanks the support from FONDECYT project 1190485. M.C. and L.S.C. are thankful for support from the project CONICYT+PAI/Atracción de Capital Humano Avanzado del Extranjero (Folio PAI80160057). L.S.C. acknowledges financial support from the Universidad Nacional de La Plata (Programa de Incentivos G11/137), the CONICET (PIP 0177), and the Agencia Nacional de Promoción Científica y Tecnológica (Préstamo BID, PICT 2016/1971), Argentina. R.O.J.V. is thankful for financial support from the UNLP under program PPID/G004. This project has received funding from the European Union's Framework Programme for Research and Innovation Horizon 2020 (2014–2020) under the Marie Skłodowska-Curie grant Agreement No. 823734.

Software: HYDWIND (Curé 2004), CMFGEN (Hillier 1990; Hillier & Miller 1998; Hillier & Lanz 2001), TLUSTY (Hubeny & Lanz 1995), FASTWIND (Santolaya-Rey et al. 1997; Puls et al. 2005).

Appendix
FASTWIND Spectra

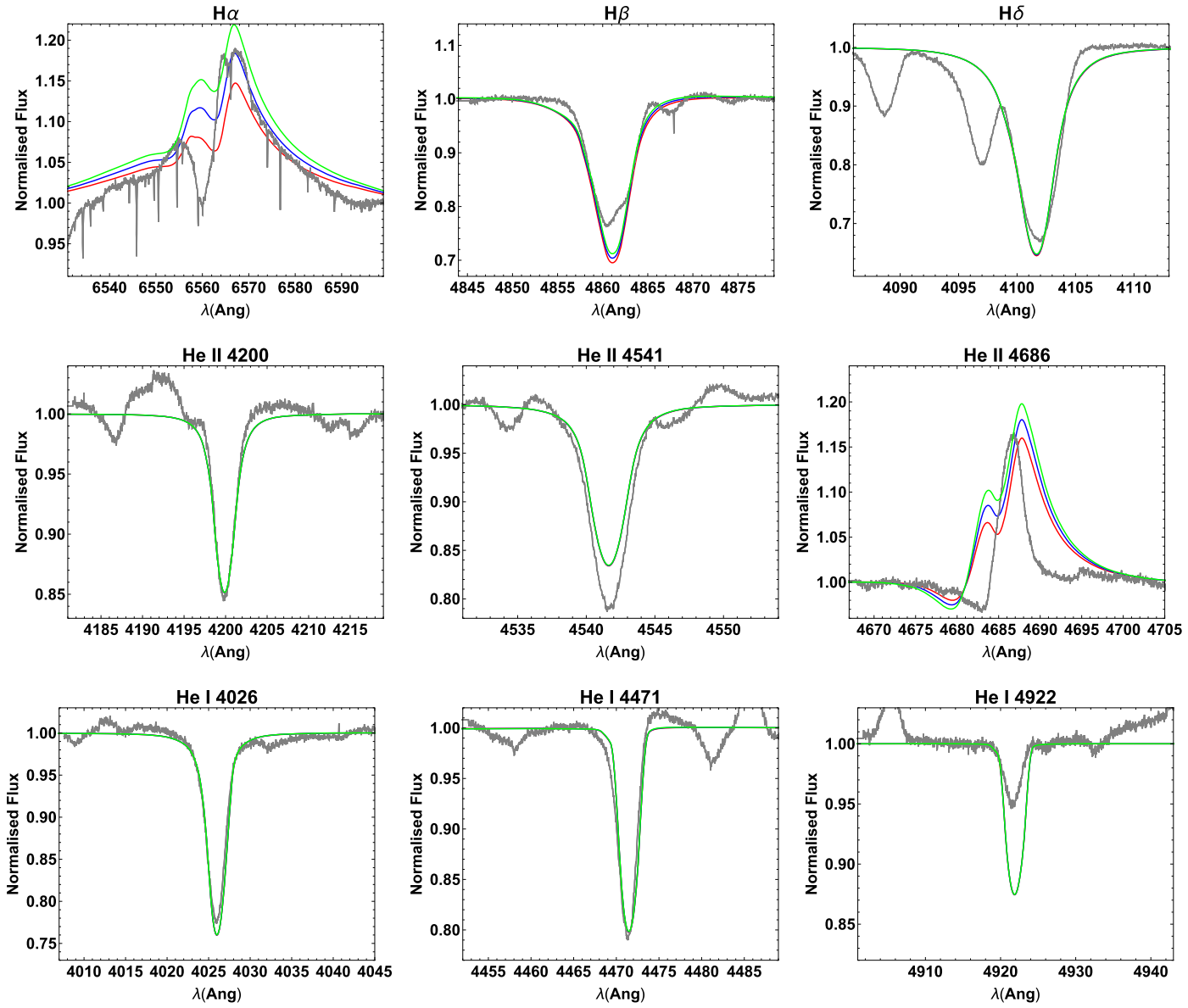

Figure 10. Resulting FASTWIND spectra for HD 163758 with $T_{\rm eff} = 34.5$ kK, log $g = 3.41$, $R_*/R_\odot = 21.0$ (see Bouret et al. 2012), and $\dot{M} = 3.3 \times 10^{-6}\ M_\odot\ {\rm yr}^{-1}$. Clumping factors are $f_{\rm cl} = 5.0$ (red), $f_{\rm cl} = 6.0$ (blue), and $f_{\rm cl} = 7.0$ (green).

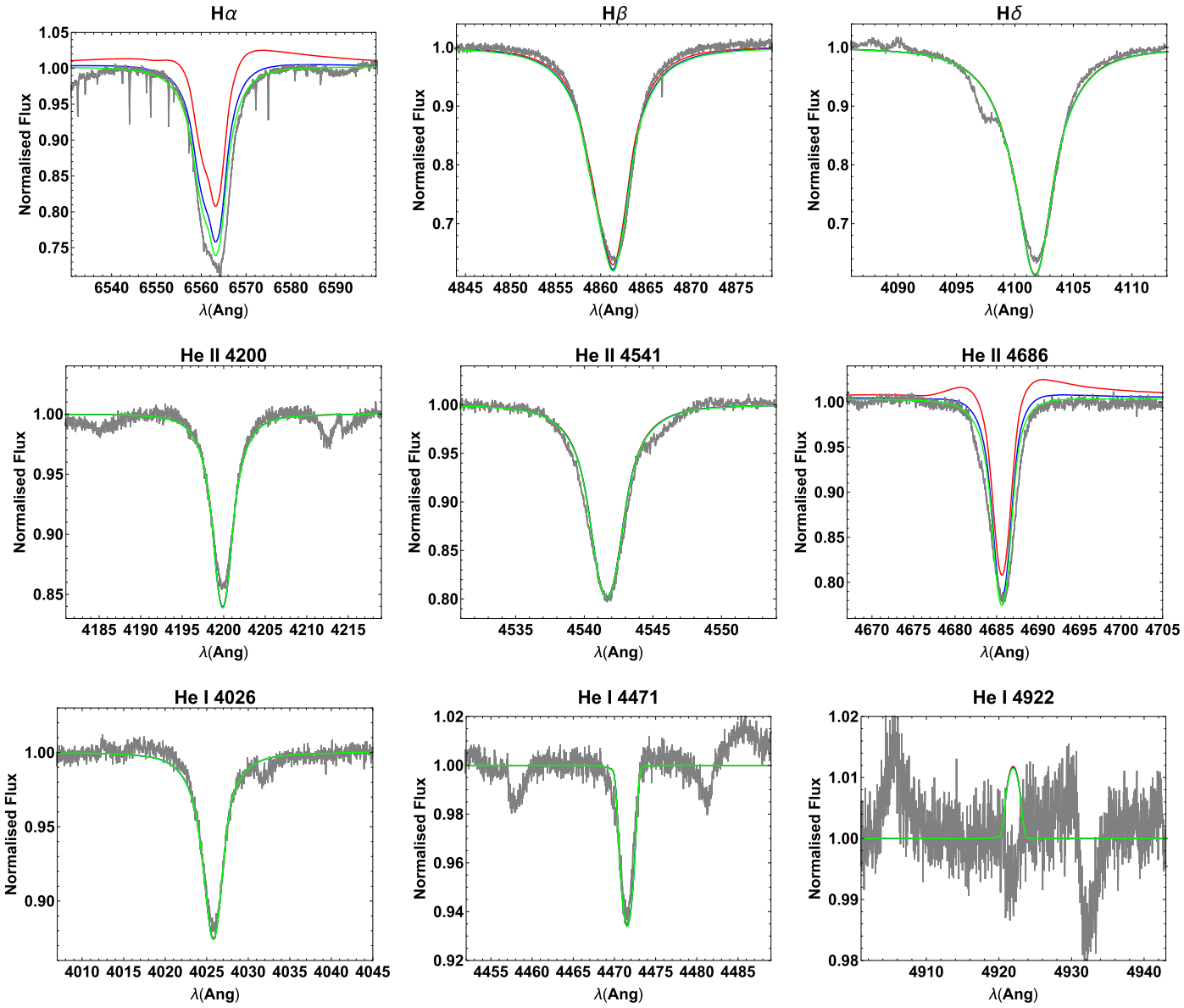

Figure 11. Resulting FASTWIND spectra for HD 164794 with $T_{\rm eff} = 43.8$ kK, $\log g = 3.92$, $R_*/R_\odot = 13.1$ (stellar parameters taken from Krtička et al. 2015), and $\dot{M} = 2.3 \times 10^{-6}\, M_\odot\, {\rm yr}^{-1}$. Clumping factors are $f_{\rm cl} = 5.0$ (red), $f_{\rm cl} = 2.0$ (blue), and $f_{\rm cl} = 1.0$ (homogeneous, green).

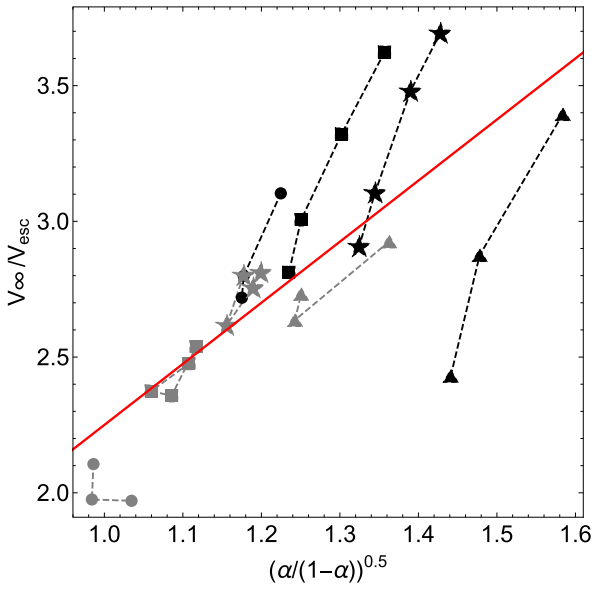

Figure 12. $v_\infty/v_{\rm esc}$ vs. $\sqrt{\alpha/(1-\alpha)}$. For each set of log g values there is a linear dependence for $Z_\odot$. Slope 2.25 of Equation (18) is also displayed. For subsolar abundance there is a unique linear relationship (see the text for details). Symbol description is the same as that in Figure 5.

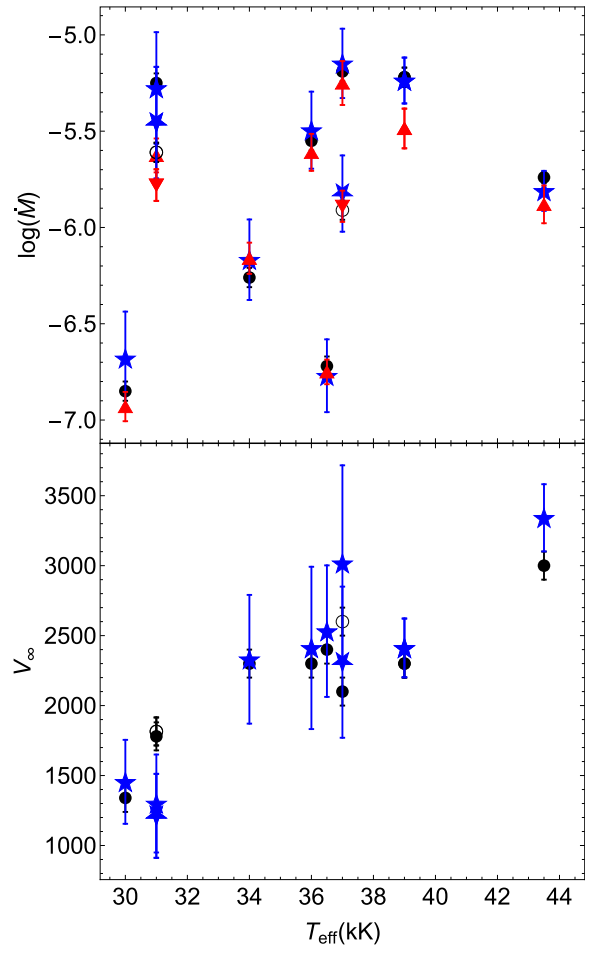

Figure 13. Comparison of mass-loss rates (upper panel) and terminal velocities (lower panel) as a function of the effective temperature. Blue stars correspond to results from this work, black disks to Bouret et al. (2005) and Markova et al. (2018) results, and red triangles to theoretical values from Vink et al. (2000). The same color code but with modified symbols (inverted blue stars, unfilled black circles, and inverted red triangles) are used to represent Markova's stars with the same effective temperature but higher surface gravity.

ORCID iDs

Alex C. Gormaz-Matamala https://orcid.org/0000-0002-2588-2391
M. Curé https://orcid.org/0000-0002-2191-8692
L. S. Cidale https://orcid.org/0000-0003-2160-7146
R. O. J. Venero https://orcid.org/0000-0001-5665-9814

References

Abbott, D. C. 1982, ApJ, 259, 282
Abbott, D. C., & Lucy, L. B. 1985, ApJ, 288, 679
Asplund, M., Grevesse, N., Sauval, A. J., & Scott, P. 2009, ARA&A, 47, 481
Bouret, J.-C., Hillier, D. J., Lanz, T., & Fullerton, A. W. 2012, A&A, 544, A67
Bouret, J.-C., Lanz, T., & Hillier, D. J. 2005, A&A, 438, 301
Cardona, O., Martínez-Arroyo, M., & López-Castillo, M. A. 2010, ApJ, 711, 239
Castor, J. I., Abbott, D. C., & Klein, R. I. 1975, ApJ, 195, 157
Castor, J. L. 1974, MNRAS, 169, 279
Curé, M. 2004, ApJ, 614, 929
Curé, M., Cidale, L., & Granada, A. 2011, ApJ, 737, 18
Fierro-Santillán, C. R., Zsargó, J., Klapp, J., et al. 2018, ApJS, 236, 38
Friend, D. B., & Abbott, D. C. 1986, ApJ, 311, 701
Hillier, D. J. 1990, A&A, 231, 116
Hillier, D. J., & Lanz, T. 2001, in ASP Conf. Ser. 247, Spectroscopic Challenges of Photoionized Plasmas, ed. G. Ferland & D. W. Savin (San Francisco, CA: ASP), 343
Hillier, D. J., & Miller, D. L. 1998, ApJ, 496, 407
Hubeny, I., & Lanz, T. 1995, ApJ, 439, 875
Krtička, J., & Kubát, J. 2010, A&A, 519, A50
Krtička, J., & Kubát, J. 2017, A&A, 606, A31
Krtička, J., Kubát, J., & Krtičková, I. 2015, A&A, 579, A111
Kudritzki, R. P. 2002, ApJ, 577, 389
Kudritzki, R. P., Pauldrach, A., Puls, J., & Abbott, D. C. 1989, A&A, 219, 205
Kudritzki, R.-P., & Puls, J. 2000, ARA&A, 38, 613
Kurucz, R. L. 1979, ApJS, 40, 1
Lamers, H. J. G. L. M., & Cassinelli, J. P. 1999, Introduction to Stellar Winds, Vol. 452 (Cambridge: Cambridge Univ. Press)
Lanz, T., & Hubeny, I. 2003, ApJS, 146, 417
Lucy, L. B., & Solomon, P. M. 1970, ApJ, 159, 879
Markova, N., & Puls, J. 2008, A&A, 478, 823
Markova, N., Puls, J., & Langer, N. 2018, A&A, 613, A12
Mazzali, P. A., & Lucy, L. B. 1993, A&A, 279, 447
Meynet, G., Maeder, A., Schaller, G., Schaerer, D., & Charbonnel, C. 1994, A&AS, 103, 97
Mihalas, D. 1978, Stellar atmospheres (2nd ed.; San Francisco, CA: Freeman)
Mokiem, M. R., de Koter, A., Puls, J., et al. 2005, A&A, 441, 711
Najarro, F., Hanson, M. M., & Puls, J. 2011, A&A, 535, A32
Noebauer, U. M., & Sim, S. A. 2015, MNRAS, 453, 3120
Pauldrach, A., Puls, J., & Kudritzki, R. P. 1986, A&A, 164, 86
Pauldrach, A. W. A. 2003, RvMA, 16, 133
Puls, J. 1987, A&A, 184, 227
Puls, J., Kudritzki, R.-P., Herrero, A., et al. 1996, A&A, 305, 171
Puls, J., Markova, N., Scuderi, S., et al. 2006, A&A, 454, 625
Puls, J., Springmann, U., & Lennon, M. 2000, A&AS, 141, 23
Puls, J., Urbaneja, M. A., Venero, R., et al. 2005, A&A, 435, 669
Puls, J., Vink, J. S., & Najarro, F. 2008, A&ARv, 16, 209
Repolust, T., Puls, J., & Herrero, A. 2004, A&A, 415, 349
Sahu, M., & Blaauw, A. 1993, in ASP Conf. Ser. 35, Massive Stars: Their Lives in the Interstellar Medium, ed. J. P. Cassinelli & E. B. Churchwell (San Francisco, CA: ASP), 278
Sander, A. A. C., Hamann, W.-R., Todt, H., Hainich, R., & Shenar, T. 2017, A&A, 603, A86
Santolaya-Rey, A. E., Puls, J., & Herrero, A. 1997, A&A, 323, 488
Schaerer, D., & Schmutz, W. 1994, A&A, 288, 231
Smith, N. 2014, ARA&A, 52, 487
Sobolev, V. V. 1960, Moving envelopes of stars
Sota, A., Maíz Apellániz, J., Walborn, N. R., et al. 2011, ApJS, 193, 24
Sundqvist, J. O., & Puls, J. 2018, A&A, 619, A59
Vink, J. S., de Koter, A., & Lamers, H. J. G. L. M. 2000, A&A, 362, 295
Vink, J. S., de Koter, A., & Lamers, H. J. G. L. M. 2001, A&A, 369, 574